Master's Thesis

New Analysis Method of Blended Active Material using Hybrid Electrode Configuration

Jin Su Yoon

School of Energy and Chemical Engineering
(Battery Science and Technology)

Ulsan National Institute of Science and Technology

2021

New Analysis Method of Blended Active Material using Hybrid Electrode Configuration

Jin Su Yoon

School of Energy and Chemical Engineering
(Battery Science and Technology)

Ulsan National Institute of Science and Technology

New Analysis Method of Blended Active Material using Hybrid Electrode Configuration

A thesis/dissertation submitted to
Ulsan National Institute of Science and Technology
in partial fulfillment of the
requirements for the degree of
Master of Science

Jin Su Yoon

12/22/2020

Approved by

Advisor
Kyeong-Min Jeong

New Analysis Method of Blended Active Material using Hybrid Electrode Configuration

Jin Su Yoon

This certifies that the thesis/dissertation of Jin Su Yoon is approved.

12/22/2020

Advisor: Kyeong-Min Jeong

Hyun-Kon Song

Dong-Hwa Seo

Abstract

In this experiment, we are going to analyze the discharge performance of the blended active material by applying a new analysis method.

Previously, it is necessary to analyze the cell performance by active material weight% in order to know the optimal ratio of the blended active material. Because the effect of each blended active material cannot be separated and it is difficult to analyze each blended active material according to the experimental environment such as discharge C-rate.

Through the hybrid system, analysis of blended active material is possible. In the hybrid system, each electrode is connected in parallel like the active material in the blending electrode. So it is possible to predict the amount of current flowing through each active material in the blending electrode by measuring the amount of current flowing through each electrode in the hybrid cell by using current tester equipment.

First, when analyzing the performance of the half-cell for each active material by the conventional method, it is confirmed that performance is dependent on the effect of the electrode structure.

Second, when analyzing the performance of each hybrid cell, it is confirmed that performance of each hybrid cell is not analyzed by the conventional method and is dependent on the current distribution. This is also applied to the blending cell. The important things in the current distribution are which active material takes more currents, whether the current distribution is even and how long is the length of the flat section.

In conclusion, the guideline for designing ratio of the blended active material could be provided.

Contents

List of Figures

List of Tables

I. Introduction

For several decades, alternative energy and energy storage systems have been studied. As shown in the Figure 1, the slope of global annual consumption is increasing, so it is necessary to prepare for the rapidly increasing energy consumption.[1] And energy consumption is increasing with the development of industry and technology.

In addition, environmental pollution issues such as global warming and the corresponding Euro 6 regulation are drawing attention. Accordingly, there are efforts to reduce the amount of fossil fuel used and replace them with alternative energy in order to reduce the amount of CO_2 generated. For this, energy storage systems are becoming more and more important, of which lithium-ion batteries are receiving the most attention. Currently, lithium-ion batteries are used not only in portable electronic devices, but also in various fields such as electric vehicles (EVs), hybrid electric vehicles (HEVs) and energy storage systems (ESSs) therefore the use of lithium-ion batteries is increasing.

In accordance with this market trend, lithium-ion batteries are being researched and the main research direction is increasing capacity and energy density. Accordingly, battery materials, electrolytes and electrode designs are being researched and active materials are often blended.

The reason for blending the active material is to increase the capacity and energy density, as well as to obtain the characteristics of each active material required according to the application.[2] For example, when blending NCA and LMO, storage life is worse than when only NCA is used but has advantages in cost, energy, power density and safety.[3] In addition, high temperature storage performance is obtained by blending NCM and Li-Mn spinel.[4] And high power density is obtained by blending NCM and activated carbon that has only adsorption reaction, not a Li intercalation material.[5]

There are many studies on active material blending, but no one can accurately analyze the effect of each active material in blending electrode. Thus it is necessary to analyze the cell performance by active material weight% to know the optimal ratio of blended active material as shown in Figure 2. Because the effect of each active material in the blended electrode cannot be accurately analyzed. For example, before the 10C-rate in Figure 3, the tendency of the discharge performance of the cell does not meet with the ratio of AC and NCM. Not only the overall effect by weight% of the active material but also the characteristics of each active material according to C-rate are different. In a conventional method, the effect of each blended active material cannot be separated and analysis according to the experimental environment such as discharge C-rate is difficult. In other words, the conventional analysis method of

blended active material has a disadvantage in that it is impossible to analyze each active material in an electrode.

However, if the hybrid system is used, analysis of blended active materials is possible. In the hybrid system, each electrode is connected in parallel like the active material in the blending electrode. In addition, it is possible to predict the amount of current flowing through each active material in the blending electrode by measuring the amount of current flowing through each electrode in the hybrid cell using current tester equipment. If this method is used, it will be very helpful in the analysis of blended active material and furthermore, it will be able to provide guidelines for designing of blended active material.

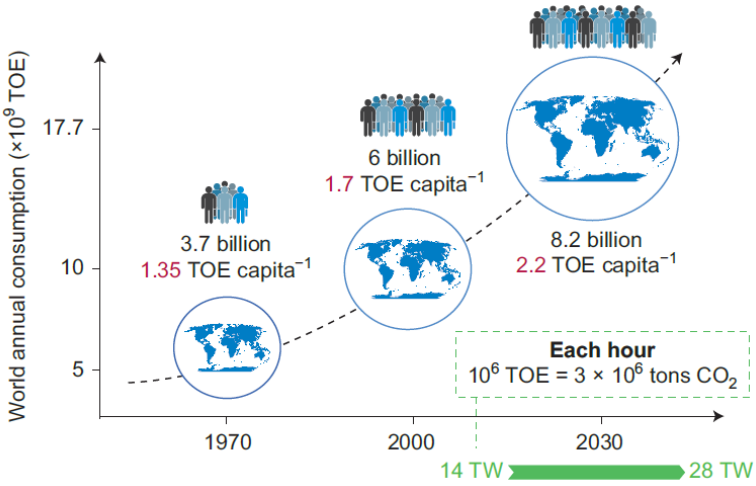

Figure 1. Past, recent and forecast of the world's energy needs up to 2050.[1]

(a) Electrodes composition and thickness.

	Electrode A	Electrode B	Electrode C	Electrode D
LFP (wt%)	85	0	65	20
AC (wt%)	0	85	20	65
Super-P (wt%)	10	10	10	10
CMC (wt%)	5	5	5	5
Thickness (μm)	17	34	21	32

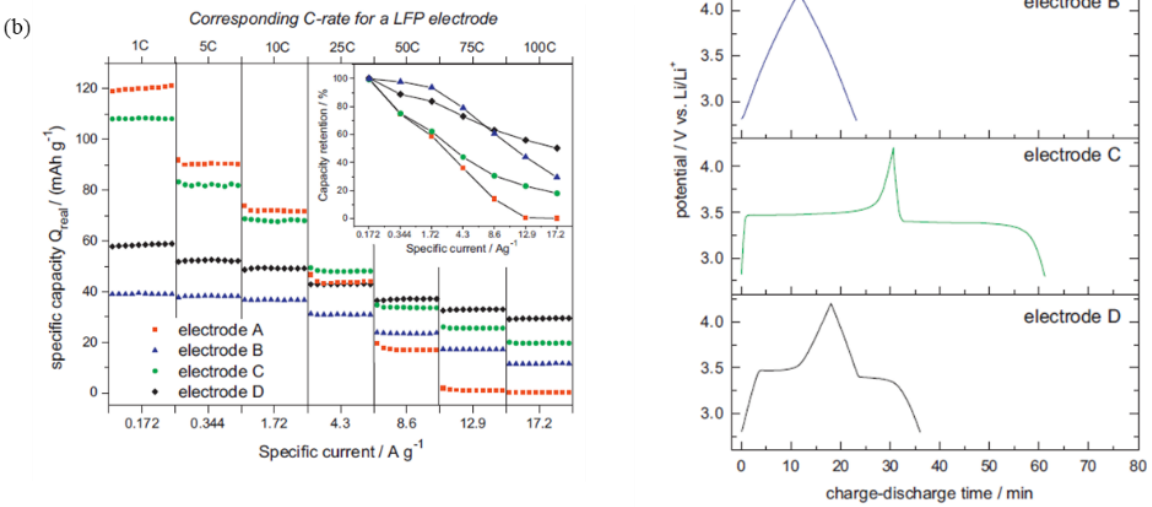

Figure 2. (a) Electrodes composition and thickness, (b) Discharge capacity of electrodes A, B, C and D, (c) Potential profiles of electrode A, B, C and D.[6]

Table 1. Composition of composite cathodes and the hybrid devices. [5]

Sample	*r* value	m_{AC} (mg)	m_{NCM} (mg)	$m_{cathode}$ (mg)	Thickness of cathode (μm)	$m_{graphite}$ (mg)	$(m_{AC} + m_{NCM})/m_{graphite}$	$m_{NCM}/m_{graphite}$	Specific current at 1C (mA g^{-1})
A10	0	31.12	0	31.12	50 ± 1	61.09	0.51	0	17.48
A31	0.25	33.41	11.14	44.55	30 ± 1	59.78	0.75	0.19	26.94
A21	0.33	33.98	16.74	50.72	65 ± 1	61.59	0.82	0.27	35.49
A11	0.50	23.89	23.89	47.78	60 ± 1	63.19	0.76	0.38	52.32
A12	0.67	19.69	39.97	59.66	50 ± 1	63.58	0.94	0.63	70.40
A13	0.75	15.45	46.35	61.80	40 ± 1	67.10	0.92	0.69	84.14
A01	1	0	66.86	66.86	29 ± 1	62.97	1.06	1.06	125.64

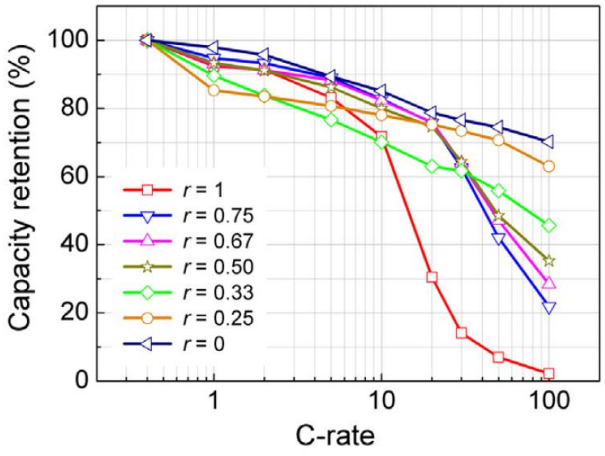

Figure 3. Rate performance as the ratio of NCM and AC.[5]

II. Experimental

2.1 Hybrid, Blended Electrode configuration

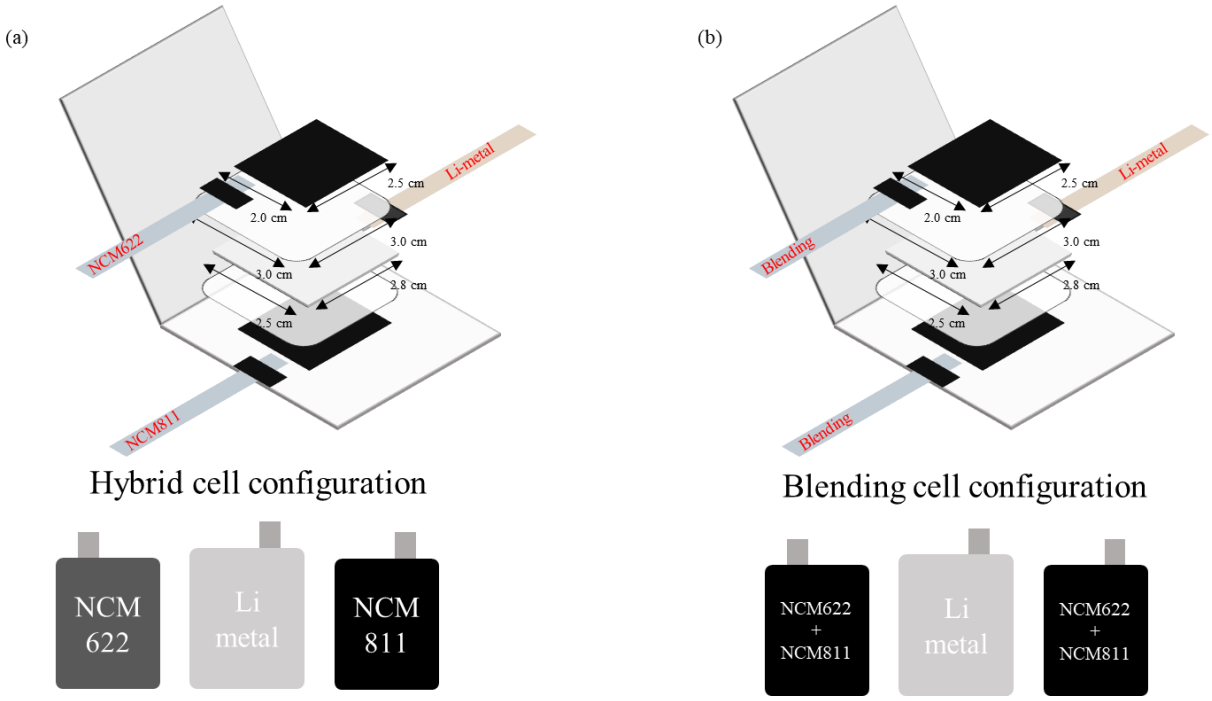

Figure 4. (a) Hybrid cell configuration, (b) Blending cell configuration.

A stack cell is fabricated using one anode and two cathodes. Conventional stack cells connect the same electrode in parallel in a stacking method, but Figure 4 shows the hybrid electrode configuration (Hybrid system, Hybrid cell) refers to a cell in which two electrodes with different active materials are connected in parallel in a stacking method. Blended electrode configuration (Blending system, Blending cell) refers to a cell in which same electrodes with blended active materials are connected in parallel in a stacking method. In the hybrid cell, electrodes made with each active material are connected in parallel, which is considered to reflect the situation that each active material is connected in parallel in the blending electrode. In other words, it reflects the voltage is the same, but the amount of current is different.

The reason that the blending cell is also fabricated as a stack cell in this experiment is to have the same influence on the structural aspects of the hybrid cell. The reason for connecting the tabs to each of the two cathodes is to use current tester equipment. In order to accurately measure the amount of current flowing through each electrode, the tabs of the two cathodes are divided so that there is no contact with each other.

2.2 Current tester equipment

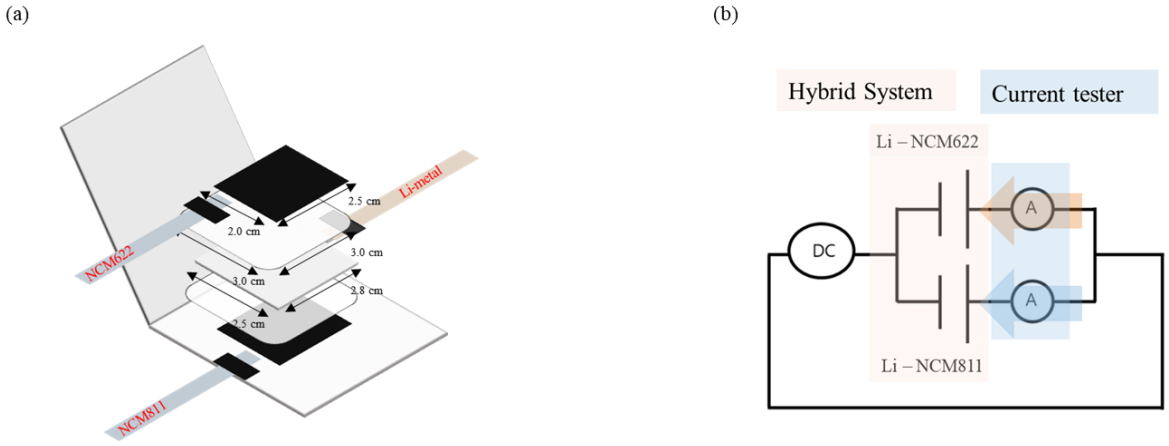

Figure 5. (a) Hybrid cell configuration, (b) Block diagram of current tester.

Current tester equipment is a device that can measure the amount of current flowing through each electrode in the hybrid cell. This equipment is a type of ammeter that measures the current flowing through the tap connected to each electrode. When making a hybrid cell, the tabs for each electrode must be connected outside and the tabs must be electrically disconnected to use this equipment. In this experiment, taps are connected to each two cathodes and the current flowing through each cathode is measured. The current flowing through the cell is applied through a cycler and the amount of current flowing in inverse proportion to the resistance of each electrode is measured through a current tester.

Cycler (PNE solution, PESC05-0.1) equipment is used to charge and discharge the cells. Electrochemical impedance spectroscopy (EIS) is performed using VSP-300, Biologic EC-Lab equipment and is tested at 100% SOC and the conditions are 5mV, 0.05Hz-1MHz. Electronic conductivity is measured by using HIOKI, (RM2610).

2.3 Design of experiments

Table 2. (a) Design of experiments, (b) Variables of x, y.[7]

(a)

Factor	Cathode	Solvent (EMC ratio)	Constraint(Energy density)	
			LL.	Density
Level	NCM622	1.15M $LiPF_6$, EC/EMC/DMC(v/v) = 2/6/2, VC 1wt.%, FEC 1wt.%, $LiPO_2F_2$ 1wt.% (EL60)	23.86	3.51
		1.15M $LiPF_6$, EC/EMC/DMC(v/v) = 2/4/4, VC 1wt.%, FEC 1wt.%, $LiPO_2F_2$ 1wt.% (EL40)	22.84	3.47
		1.15M $LiPF_6$, EC/EMC/DMC(v/v) = 2/1/7, VC 1wt.%, FEC 1wt.%, $LiPO_2F_2$ 1wt.% (EL10)	22.91	3.44
	NCM811	60% (EL60)	21.18	3.31
		40% (EL40)	21.39	3.34
		10% (EL10)	21.28	3.34
	Blending	40% (EL40)	23.28	3.27
			23.18	3.26

(b)

x	Electrode component (NCM622, NCM811) Half-cell	System (Hybrid, blending) Stack-cell
y	Rate capability (Cap vs. 0.2C Cap) Power density (V_{avg} → P_{avg}) Effective ionic conductivity (κ_{eff}) Ratio of the ohmic and the kinetic resistance (v^2) Ratio of the conductivity of the electrolyte (κ) to that of the solid matrix (σ). (K_r)	

In the experiment, NCM622 and NCM811 are used as cathodes. The half-cell, hybrid cell and blending cell are fabricated using Li metal as an anode electrode. Electrolyte is 1.15M $LiPF_6$, EC/EMC/DMC = 1/3/1, VC 1wt%., FEC 1wt%., $LiPO_2F_2$ 1wt%. (EL60), 1.15M $LiPF_6$, EC/EMC/DMC = 2/4/4, VC 1wt%., FEC 1wt%., $LiPO_2F_2$ 1wt%. (EL40), 1.15M $LiPF_6$, EC/EMC/DMC = 2/1/7, VC 1wt%., FEC 1wt%., $LiPO_2F_2$ 1wt%. (EL10). They are named EL60, EL40 and EL10 according to the ratio of EMC in the electrolyte solvent composition. The separator is composed of PE. Each electrode is fabricated to compare the power density performance at the same energy density.

The values are measured such as rate capability, power density, effective ionic conductivity (κ_{eff}), the ratio of the ohmic and the kinetic resistance (v^2), the ratio of the conductivity of the electrolyte (κ) to that of the solid matrix (σ), (K_r) according to electrode component type and cell system.

III. Results and discussion

3.1 Bulk ionic conductivity

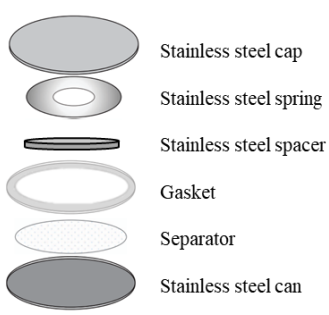

Figure 6. SUS symmetric cell configuration.

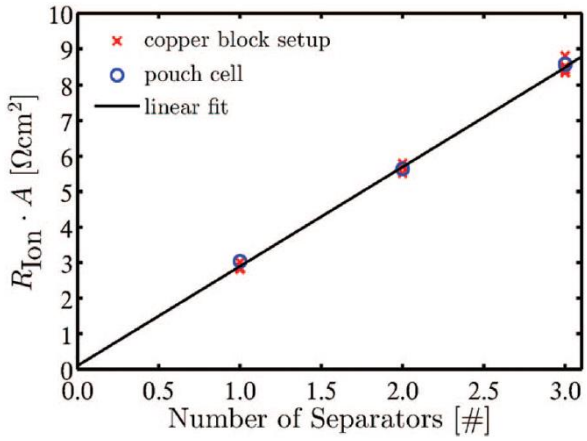

Figure 7. High frequency areal resistance of multiple layers of Celgard 2325 separators soaked with 1MLiPF6 in EC:EMC (3:7 w:w) + 2% VC using both the copper block setup (four repeat experiments per stacking) and pouch cells (one experiment per stacking).[8]

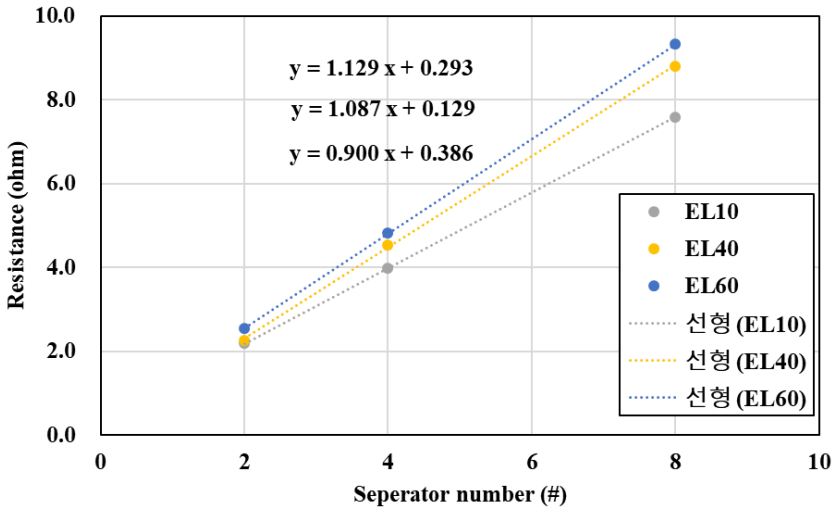

Figure 8. High frequency resistance of Celgard 2320 separators with each electrolyte.

$$\kappa_{eff} = \frac{\varepsilon}{\tau}\ \kappa_{bulk} \ldots (1)$$

Table 3. (a) Information of separator, (b) Resistance, effective and bulk ionic conductivity.[9]

(a)

Celgard 2320	16 pi	Separator th
	2.011cm^2	0.002cm/#

(b)

	2	4	8	R(ohm)	κ_{eff}(mS/cm)	ε_{sep}	τ_{sep}	κ_{bulk}(mS/cm)
EL10	2.182	3.990	7.582	0.900	1.106	0.39	3.9	11.056
EL40	2.257	4.543	8.799	1.087	0.916	0.39	3.9	9.155
EL60	2.546	4.816	9.321	1.129	0.881	0.39	3.9	8.812

κ_{eff} is effective ionic conductivity, κ_{bulk} is bulk ionic conductivity, ε is porosity τ is tortuosity. First, the bulk ionic conductivity of each electrolyte solvent composition is measured. In Figure 6, symmetric cell made with SUS electrodes is fabricated and the EIS resistance is measured by changing the number of separators in the cell. The reason for using the SUS electrode is to measure only the resistance due to Li^+ movement by making a blocking condition without a charge transfer. Because of blocking condition, the resistance depends on the number of separators. Figure 8 and Table 3 show when the resistance for each number of separators is linearly fitted, the slope represents the effective ionic conductivity of one separator and κ_{bulk} is calculated using the porosity (ε) and tortuosity (τ) of the separator and Eqn. (1). Porosity and tortuosity of Celgard 2320 separator is 0.39, 3.9. The ionic conductivity is EL10: 11.056, EL 40: 9.155 and EL 60: 8.812 mS/cm. As the EMC ratio decreases, in other words, the DMC ratio increases, the ionic conductivity tends to increase because the ionic conductivity of DMC is greater than that of EMC.

3.2 Effective ionic conductivity

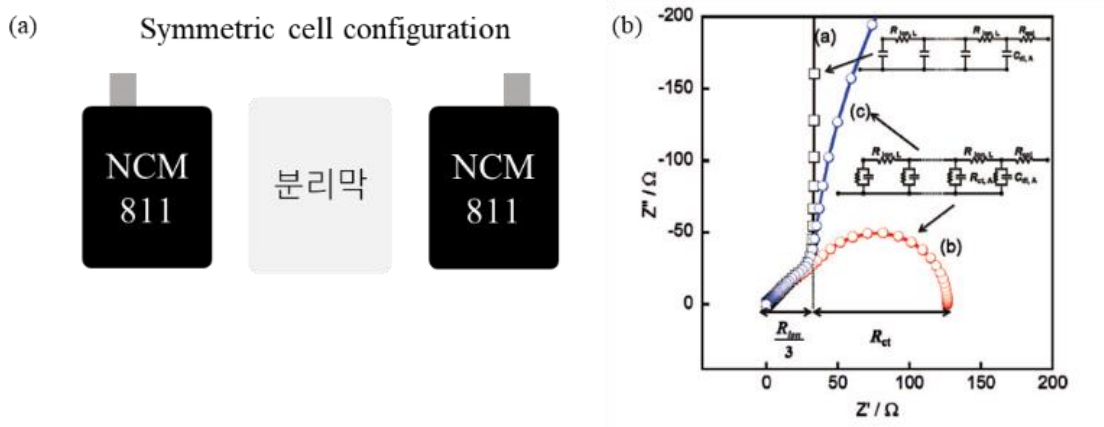

Figure 9. (a) Symmetric cell configuration, (b) EIS of symmetric cell.[10]

$$R_{ion} = \frac{L}{\kappa_{eff} A} \dots (2)$$

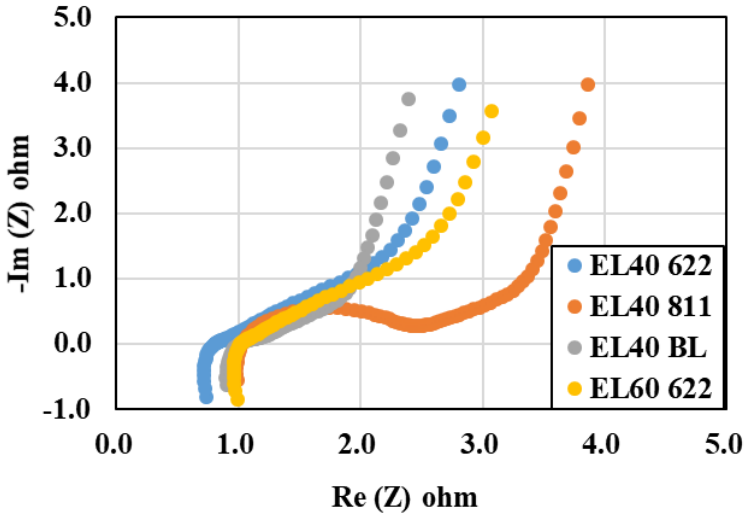

Figure 10. EIS of each symmetric cell.

Table 4. Effective ionic conductivity of each electrode and electrolyte.

Electrode	EL10 811	EL40 811	EL60 811	EL10 622	EL40 622	EL60 622
κ_{eff}(mS/cm)	0.90	0.74	0.71	0.73	0.60	0.52

R_{ion} is the ionic resistance in pores, κ_{eff} is the effective ionic conductivity, L is the sum of the lengths of the two electrodes and A is the area of the electrode.

Figure 9 (b) shows R_{ion} is measured after fabricating symmetric cell for each electrode. R_{ion} is the resistance generated when Li^+ moves within the electrode pores. Using Eqn. (2), the effective ionic conductivity (κ_{eff}) in the electrode is calculated. By applying the effective ionic conductivity and the bulk ionic conductivity of the electrolyte to Eqn. (1), the ratio of the porosity and tortuosity of the electrode is calculated and the effective ionic conductivity of each electrode is calculated. The values are shown in Table 4. It is confirmed that the effective ionic conductivity is affected by the bulk ionic conductivity of the electrolyte and the structural factor of the electrode.

3.3 Dimensionless current density

Dimensionless parameter is calculated to know the distribution of current density in the electrolyte in the thickness direction of the electrode. Equations are derived to know the exact meaning of the dimensionless current density. This part is cited in the 1st edition of electrochemical engineering.[11] The assumptions of the equation are neglecting concentration gradients, steady-state and linear kinetics.

$$-\nabla \cdot i_2 + ai_n = 0 \ldots (3)$$

$$\frac{di_2}{dx} = \frac{ai_0(\alpha_a+\alpha_c)F}{RT}(\phi_1 - \phi_2) \ldots (4)$$

First, the governing equation is derived using the charge balance and the modified butler-volmer equation according to linear kinetic.

$$\frac{d^2 i_2}{dx^2} = \frac{ai_0(\alpha_a+\alpha_c)F}{RT}\left(\frac{i_2 - {}^{I}/_{A}}{\sigma} + \frac{i_2}{\kappa}\right) \ldots (5)$$

This equation is an ordinary differential equation with i_2 as the only unknown. Dimensionless parameters are used like the following equations.

$$i^* \equiv \frac{i_2}{{}^{I}/_{A}} \ldots (6)$$

$$z \equiv \frac{x}{L} \ldots (7)$$

$$v^2 \equiv \frac{ai_0(\alpha_a+\alpha_c)FL^2}{RT}\left(\frac{1}{\sigma} + \frac{1}{\kappa}\right) \ldots (8)$$

$$K_r \equiv \frac{\kappa}{\sigma} \ldots (9)$$

Second order, ordinary differential equation can be solved analytically to yield i* as a function of z.

$$\frac{\mathrm{d}^2 i^*}{\mathrm{dz}^2} = v^2 \left(\mathrm{i}^* - \frac{K_r}{1+K_r} \right) \ldots (10)$$

Two boundary conditions are used.

$$i_2 = {}^{I}/_{A} \quad at \quad x = L; \quad i^* = 1 \; at \; z = 1 \ldots (11)$$

$$i_2 = 0 \quad at \quad x = 0; \quad i^* = 0 \; at \; z = 0 \ldots (12)$$

Solution is

$$i^* = \frac{K_r}{1+K_r} + \frac{\sinh(vz)+K_r sinh(v(z-1))}{(1+K_r)\sinh(v)} \ldots (13)$$

Figure 11 shows the dimensionless current density is a value representing the distribution of the current density in the thickness direction of the electrode. This represents the uniformity of the current distribution within the electrode.

This current density can be differentiated to give a dimensionless local reaction rate.

$$\frac{di^*}{dz} = \frac{vcosh(vz)+vK_r cosh(v(z-1))}{(1+K_r)\sinh(v)} \ldots (14)$$

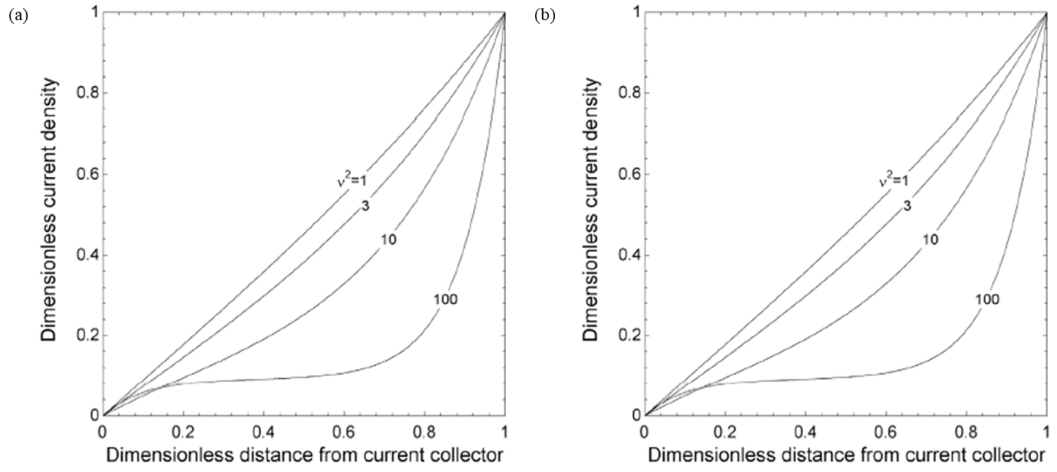

Figure 11. (a) Dimensionless current density, (b) Derivative of (a), across the electrode. K_r = 0.1[11]

K_r and v^2 are important parameters. K_r represents the ratio of the conductivity of the electrolyte (κ) to that of the solid matrix (σ). When K_r increases, it has symmetric current density distribution and vice versa. Figure 11 shows v^2 represents the ratio of the ohmic and the kinetic resistance.

When v^2 rises, kinetic resistance is dominant and current density distribution is uniform. In the opposite case, ohmic resistance is dominant and current density distribution is non-uniform. If the current density distribution is uniform, good discharge performance can be expected.

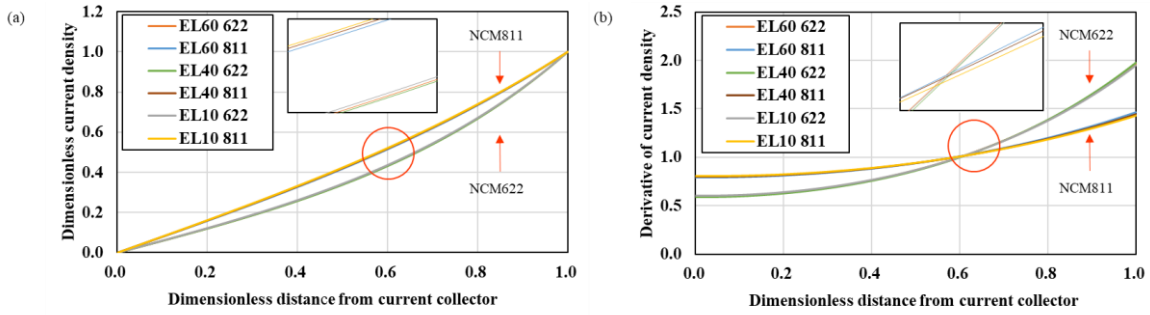

Figure 12. (a) Dimensionless current density, (b) Derivative of (a), across the electrode.

Table 5. v^2, K_r of each electrode and electrolyte.

	EL60		EL40		EL10	
	622	811	622	811	622	811
v^2	3.54	1.58	3.60	1.50	3.48	1.45
K_r	5.63E-03	1.56E-02	6.60E-03	1.57E-02	8.12E-03	1.90E-02

Figure 12 shows the analysis of dimensionless current density is applied to the half-cell used in this experiment. Table 5 shows the v^2 value of NCM622 is larger than that of NCM811. From this, it can be concluded that NCM622 is more dominant in ohmic resistance than NCM811 and NCM622 has a non-symmetric current density distribution than NCM811 through K_r. This can be confirmed again through the graph of the dimensionless current density and derivative of the current density. Since the current density of NCM622 is non-uniform and non-symmetric than that of NCM811, the discharge performance of NCM622 will be lower than that of NCM811.

3.4 Discharge performance

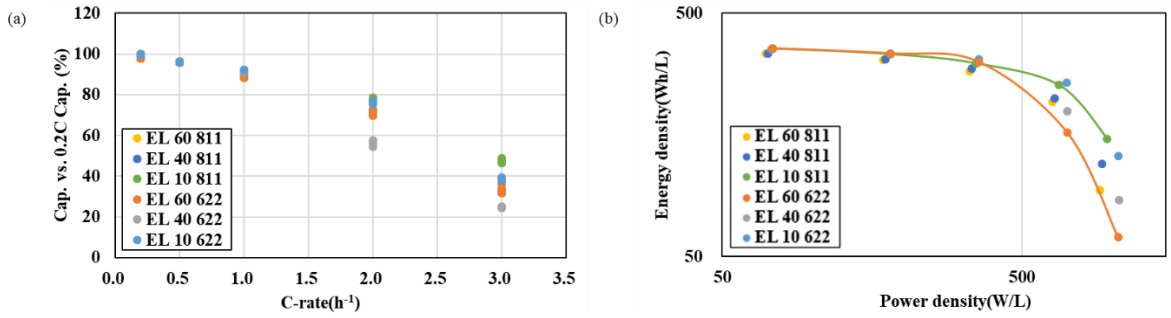

Figure 13. (a) Rate capability of NCM622, NCM811, (b) Ragone plot of NCM622, NCM811.

Table 6. Order of discharge performance, effective ionic conductivity of each electrode and electrolyte.

Performance	1	2	3	4	5	6
Cell	EL10 811	EL10 622	EL40 811	EL60 811	EL40 622	EL60 622
κ_{eff}(mS/cm)	0.90	0.73	0.74	0.71	0.60	0.52

The discharge performance of each half-cell is compared at the same energy density. The composite density of NCM622 is higher than that of NCM811 to make the same energy density. The discharge performance is shown in Figure 13. The Table 6 shows the order of discharge performance and the effective ionic conductivity. Through this, it is confirmed that the discharge performance of the half-cell is dependent on the effective ionic conductivity. The discharge performance increases due to decrease in iR drop, concentration overpotential and surface overpotential as effective ionic conductivity increases.

$$\lambda_i = \frac{|z_i|F^2 D_i}{RT}\ ,\ \Lambda = \lambda_+ + \lambda_- = \frac{\kappa}{c} \quad \dots (15)$$

$$i_0 = i_{0,ref}\left(\frac{c_1}{c_{1,ref}}\right)^{\gamma_1}\left(\frac{c_2}{c_{2,ref}}\right)^{\gamma_2} \dots (16)$$

$$i = i_0\left[\exp\left(\frac{\alpha_a F \eta_s}{RT}\right) - \exp\left(-\frac{\alpha_c F \eta_s}{RT}\right)\right] \dots (17)$$

λ_i is equivalent conductance, z_i is charge number, F is Faraday's constant, R is gas constant, T is the absolute temperature, D_i is solution diffusion coefficient, Λ is conductance, κ is ionic conductivity, c is salt concentration, i_o is exchange current density, $i_{o,ref}$ is exchange current density(ref), α_a, α_c is transfer coefficient for anodic and cathodic reactions, η_S is surface overpotential.

The reason why the discharge performance is affected by the effective ionic conductivity is that the solution diffusion coefficient increases as the effective ionic conductivity increases (Eqn. 15). Then concentration overpotential decreases. Also, as the solution diffusion coefficient increases, c_1 and c_2 increase (Eqn. 16). Then i_0 increases. Since i is constant, the surface overpotential(η_s) decreases (Eqn. 17). In other words, as the effective ionic conductivity increases, the iR drop, the concentration overpotential and the surface overpotential decreases, so the discharge performance increases.

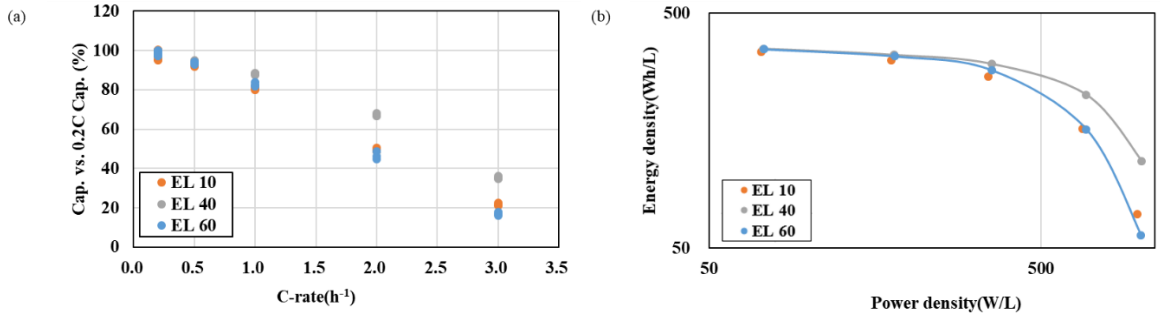

Figure 14. (a) Rate capability of each hybrid cell, (b) Ragone plot of each hybrid cell.

Table 7. Effective ionic conductivity of each hybrid cell.

	EL10		EL40		EL60	
Electrode	622	811	622	811	622	811
κ_{eff}(mS/cm)	0.73	0.90	0.60	0.74	0.52	0.71

Figure 14 shows the compared discharge performance of each hybrid cell. The discharge performance of EL40 is best and EL60 is worst. However, effective ionic conductivity of EL10 is best and EL60 is worst in Table 7.

The performance of hybrid cell does not depend on the ionic conductivity like half-cell. In other words, the conventional analysis method cannot be applied to the hybrid cell.

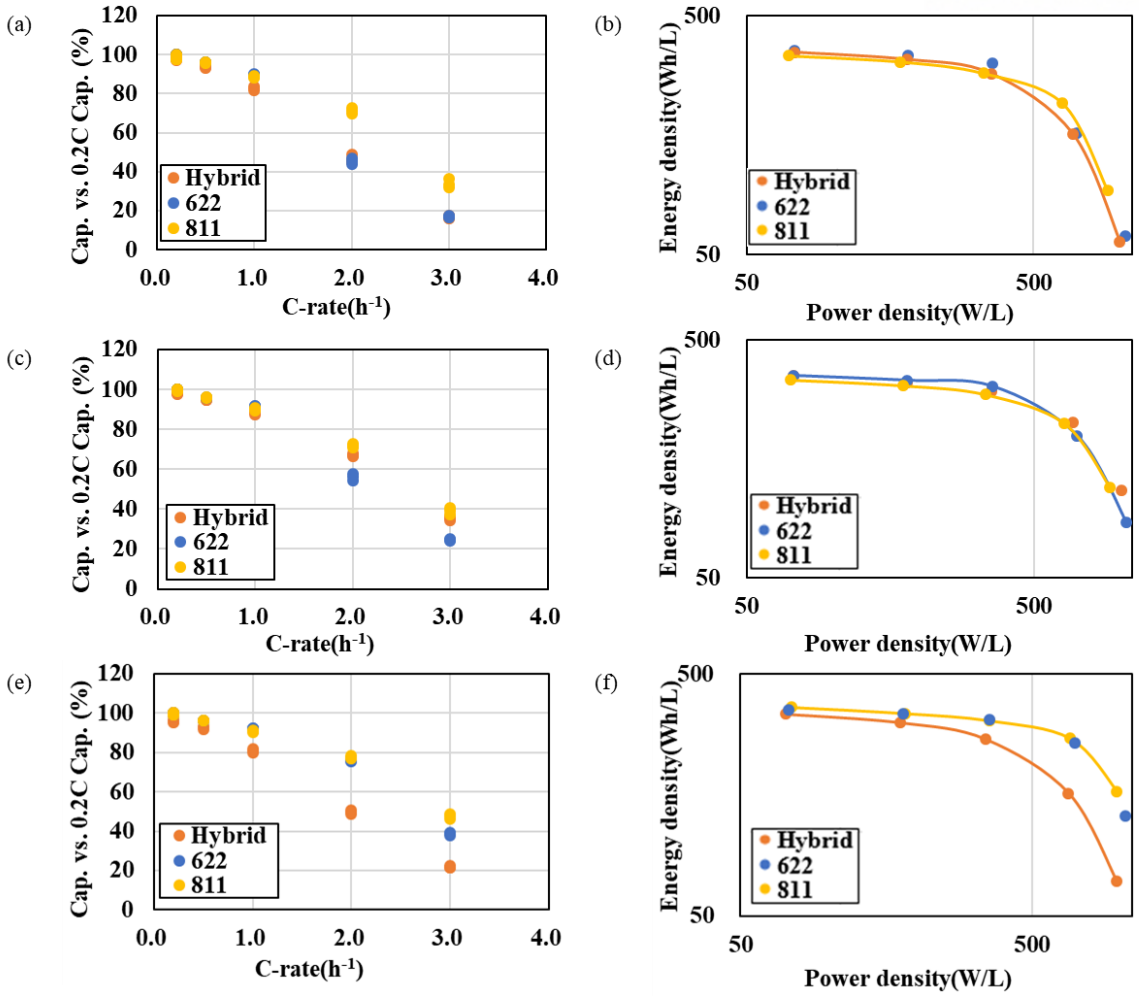

Figure 15. (a), (c), (e) Rate capability of each NCM622, NCM811, hybrid cell of each electrolyte, (b), (d), (f) Ragone plot of each NCM622, NCM811, hybrid cell of each electrolyte.

In Figure 15, the performance of the hybrid and half-cell is compared to analyze the performance of the hybrid cell. The performance of EL60 hybrid cell is low up to 1C but similar to that of NCM622 from 2C. For EL40 Hybrid cell, the discharge performance is between NCM622 and NCM811 and it is closer to NCM811. For EL10 Hybrid cell, performance is lower than that of NCM622.

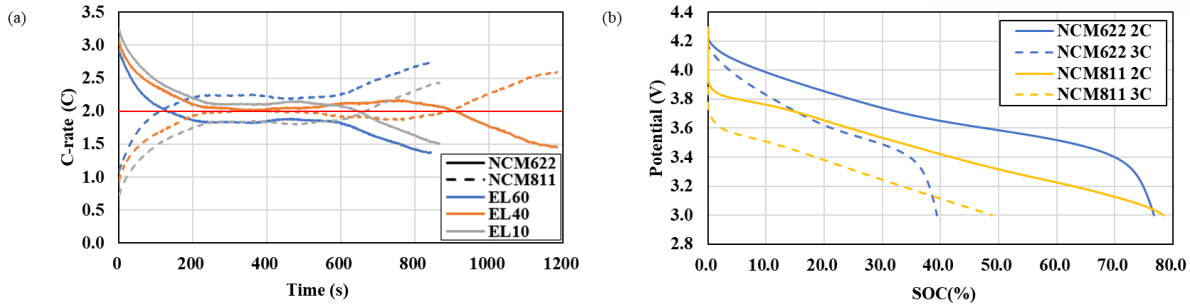

Figure 16. (a) Current distribution of each NCM622, NCM811 electrode in hybrid cell, (b) Voltage profile of NCM622, NCM811 half-cell.

The current distribution is mainly considered when analyzing the hybrid cell performance. Because the discharging performance of hybrid cells cannot be explained by conventional methods. In Figure 16 (a), the important things in current distribution are which active material takes more currents, whether the current distribution is even and how long is the length of the flat section.

The performance of EL60 Hybrid cell is similar to that of NCM622 from 2C because more currents flow through the NCM811 and the flat section is short. The performance of EL40 Hybrid cell is between NCM622 and NCM811 because current distribution is even and the length of flat section is longer. The performance of EL10 Hybrid cell is lower than that of NCM622 because flat section is short and also more currents flow through the NCM622 so performance is lower than NCM622 half-cell.

In Figure 16 (a), more currents always flow through the NCM622 initially. This means that the initial resistance of the NCM622 is smaller than that of the NCM811. The Figure 16 (b) is the discharge profile of the half-cell and the iR drop is larger in the initial NCM811. It can be seen that there is a difference in initial resistance due to the difference in intrinsic properties of the active material between NCM622 and NCM811. In the Figure 16 (a), it is regarded as the structure effect of the electrode appears from the middle of current distribution. The important things in the performance of hybrid cell is which active material takes more currents, whether the current distribution is even and how long is the length of the flat section.

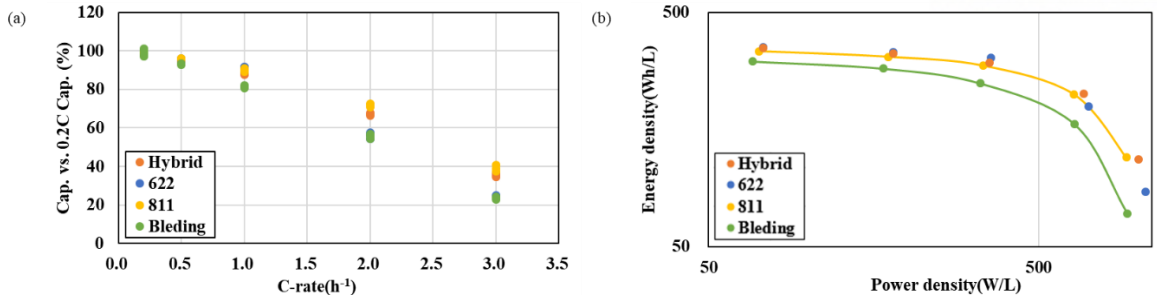

Figure 17. (a) Rate capability of each NCM622, NCM811, hybrid, blending, (b) Ragone plot of each NCM622, NCM811, hybrid, blending.

In Figure 17, the performance of NCM622, NCM811, hybrid and blending cells is compared at the same energy density. The method of evaluating the discharge performance is the same as before and Figure 17 shows the experimental result for the case of EL40 electrolyte. The order of performance is blending, NCM622, hybrid cell and NCM811. The discharge performance of blending cell is similar to that of NCM622, but it always shows the lowest performance.

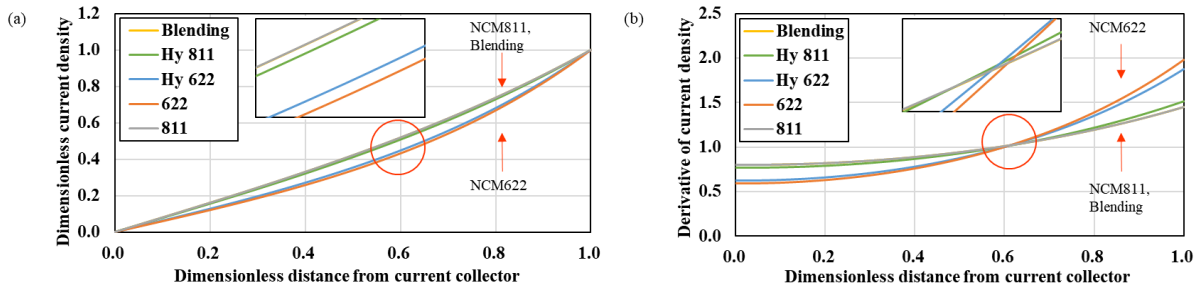

Figure 18. (a) Dimensionless current density, (b) Derivative of (a), across the electrode.

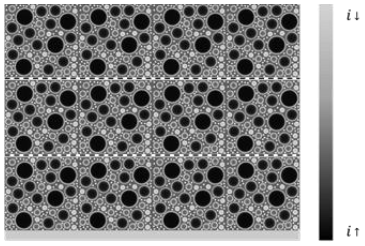

Figure 19. Schematic diagram of current distribution across the electrode.[12]

Table 8. v^2, K_r, effective ionic conductivity of each electrode and electrolyte.

	622	811	Hybrid 622	Hybrid 811	Blending
v^2	3.60	1.50	3.16	1.74	1.51
K_r	6.60E-03	1.57E-02	6.60E-03	1.57E-02	1.66E-02
κ_{eff}(mS/cm)	0.60	0.75	0.60	0.75	1.16

$$i^* = \frac{K_r}{1+K_r} + \frac{\sinh(vz) + K_r sinh(v(z-1))}{(1+K_r)\sinh(v)} \dots (13)$$

$$\frac{di^*}{dz} = \frac{vcosh(vz)+vK_r cosh(v(z-1))}{(1+K_r)\sinh(v)} \dots (14)$$

For the performance analysis of the blending cell, the analysis method is same as half-cell. First, dimensionless current density is analyzed like a half-cell. Figure 18 shows the NCM811, NCM622 electrodes in the hybrid cell shows a similar trend to the NCM811 and NCM622 of half-cell because the electrode of half and hybrid cell is the same. Blending electrode represents uniform current density distribution, like the electrode of NCM811 in half-cell and NCM811 in hybrid cell. In the case of blending, the electrode structure effect is similar to that of NCM811. However, discharge performance is the worst because this analysis method does not reflect the amount of current distribution flowing through each active material in the blending electrode. In order words, in the case of the blending electrode, the current distribution is uniform in the electrode thickness direction, but if the electrode is considered to be divided by floors, the current distribution flowing each floor to each active material in the horizontal direction cannot be known in Figure 19.

In the case of half-cell, discharge performance depends on the effective ionic conductivity. However, in the case of blending, although the effective ionic conductivity value is the highest, but the discharge performance is the worst.

The cause of the discharge performance of the blending cell appeared regardless of the effective ionic conductivity and the uniformity of the current density in the electrode of thickness direction. Since the two parameters represent the transport of lithium ions in the electrolyte and the ratio of the conductivity of the electrolyte and the solid, the difference in the amount of current flowing to each active material in the blended electrode cannot be known. As seen in the hybrid cell, when other active materials are used, the amount of current flowing through each active material must be analyzed.

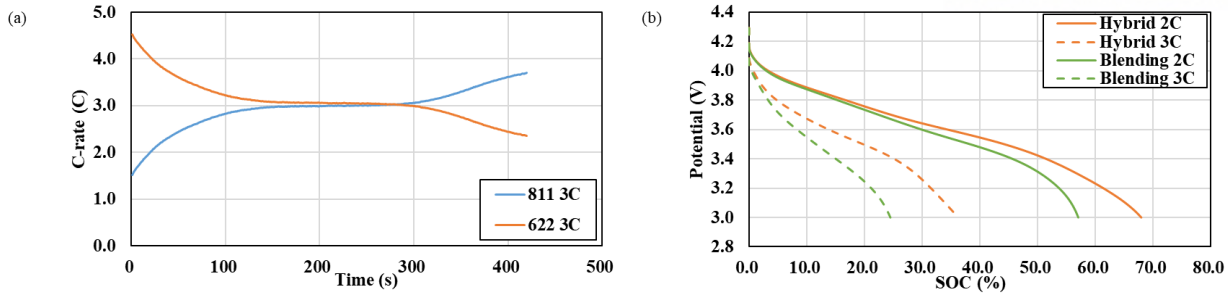

Figure 20. (a) Current distribution of hybrid cell, (b) Voltage profile of hybrid and blending cell.

Table 9. Capacity ratio of each electrode in hybrid cell with discharge C-rate.

C-rate	0.2		0.5		1.0		2.0		3.0	
Electrode	811	622	811	622	811	622	811	622	811	622
Cap. (%)	48	52	50	50	49	51	49	51	48	52

Table 10. Density and effective ionic conductivity of each electrode.

	622	811	Hybrid 622	Hybrid 811	Blending
Density	3.47	3.34	3.47	3.34	3.27
κ_{eff}(mS/cm)	0.60	0.75	0.60	0.75	1.16

The cause of discharge performance will be more currents flow through NCM622 in blending electrode. In order to analyze the performance of blending, the hybrid cell must be analyzed. Discharge performance of hybrid cell is between NCM622 and NCM811, because this hybrid cell has a long length of flat section and even current distribution in Figure 20 (a).

First, the 0.2C discharge performance of hybrid cell must be analyzed to analyze blending with hybrid cell. In this case, the effect of the electrode structure is negligible and the current distribution will be affected by the intrinsic property of the active material. Table 9 shows more currents flow through NCM622 in this case, it is possible to predict that more currents flow through NCM622 in blending.

Second, Figure 20 (b) shows discharge profile of blending, the voltage profile of blending is more similar to that of NCM622 half-cell than that of hybrid cell.

Third, Table 10 shows the composite density reduction of the NCM622 is greater than that of NCM811 when comparing the composite density of hybrid and blending. Therefore, more currents flow through NCM622 in blending as the ion conductivity increases at NCM622.

Therefore, the performance of blending is lower than that of the hybrid because more currents flow through the NCM622 in the blending.

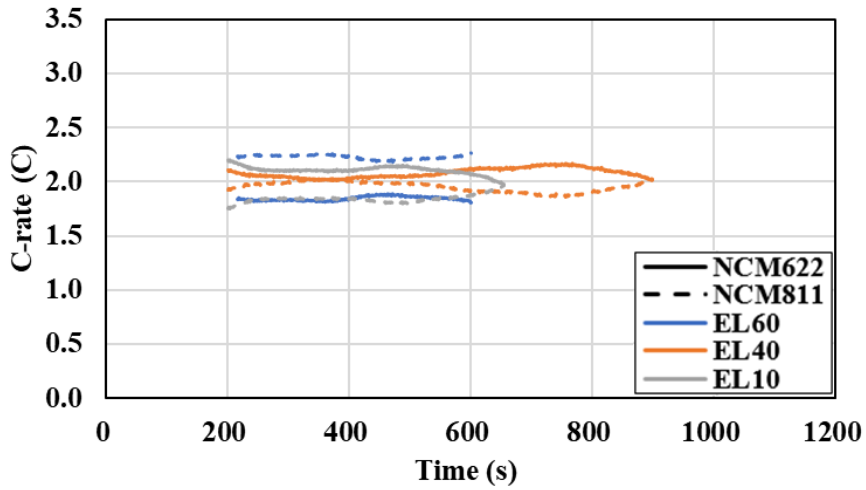

Figure 21. Current distribution and length of flat section of each electrode in hybrid cell.

In the case of using two active materials, hybrid or blending cell, the effect of the electrode structure which is important in a general half-cell is not important.

As seen in Figure 21, discharge performance is affected by which active material takes more currents, whether the current distribution is even and how long is the length of the flat section.

Therefore, it is necessary to analyze the distribution of the current density, in order to analyze the discharge performance of the blending cell.

IV. Conclusion

Like the active materials connected in parallel in the blending electrode, electrodes of hybrid cell made with each active material are connected in parallel.

The discharge performance of hybrid and blending cell is less affected by the electrode structure unlike general half-cell. Rather it is affected by which active material takes more currents, whether the current distribution is even and how long is the length of the flat section.

Therefore, it can be concluded that application of hybrid system is suitable as a new method of analyzing blended active materials. Through this, the design guideline can be provided when designing the ratio of blended active material.

V. Reference

1. Larcher, D., & Tarascon, J. M. (2015). Towards greener and more sustainable batteries for electrical energy storage. *Nature chemistry*, *7*(1), 19-29.
2. Chikkannanavar, S. B., Bernardi, D. M., & Liu, L. (2014). A review of blended cathode materials for use in Li-ion batteries. *Journal of Power Sources*, *248*, 91-100.
3. Albertus, P., Christensen, J., & Newman, J. (2009). Experiments on and modeling of positive electrodes with multiple active materials for lithium-ion batteries. *Journal of the Electrochemical Society*, *156*(7), A606.
4. Kitao, H., Fujihara, T., Takeda, K., Nakanishi, N., & Nohma, T. (2004). High-temperature storage performance of Li-ion batteries using a mixture of Li-Mn spinel and Li-Ni-Co-Mn oxide as a positive electrode material. *Electrochemical and Solid State Letters*, *8*(2), A87.
5. Sun, X., Zhang, X., Huang, B., Zhang, H., Zhang, D., & Ma, Y. (2013). (LiNi0. 5Co0. 2Mn0. 3O2+ AC)/graphite hybrid energy storage device with high specific energy and high rate capability. *Journal of power sources*, *243*, 361-368.
6. Böckenfeld, N., Placke, T., Winter, M., Passerini, S., & Balducci, A. (2012). The influence of activated carbon on the performance of lithium iron phosphate based electrodes. *Electrochimica acta*, *76*, 130-136.
7. Xiao, L. F., Cao, Y. L., Ai, X. P., & Yang, H. X. (2004). Optimization of EC-based multi-solvent electrolytes for low temperature applications of lithium-ion batteries. *Electrochimica acta*, *49*(27), 4857-4863.
8. Landesfeind, J., Hattendorff, J., Ehrl, A., Wall, W. A., & Gasteiger, H. A. (2016). Tortuosity determination of battery electrodes and separators by impedance spectroscopy. *Journal of The Electrochemical Society*, *163*(7), A1373.
9. Celgard Co. Celgard® High performance Battery Separators [Data file].
10. Ogihara, N., Kawauchi, S., Okuda, C., Itou, Y., Takeuchi, Y., & Ukyo, Y. (2012). Theoretical and experimental analysis of porous electrodes for lithium-ion batteries by electrochemical impedance spectroscopy using a symmetric cell. *Journal of The Electrochemical Society*, *159*(7), A1034.

11. Fuller, T. F., & Harb, J. N. (2018). *Electrochemical engineering*. John Wiley & Sons.

12. Ji, L., & Guo, Z. (2018). Analytical modeling and simulation of porous electrodes: Li-ion distribution and diffusion-induced stress. *Acta Mechanica Sinica*, *34*(1), 187-198.

VI. Acknowledgement

This work was supported by Hankook AtlasBX.

Special thanks to dissertation committee assistant referees, Prof. Hyun-Kon Song and Prof. Dong-Hwa Seo.

Lastly, I sincerely appreciate Prof. Kyeong-Min Jeong.